SUPPLEMENTAL MATERIAL to the paper

Supplementary Figure 1| The Wong-Wang Model. Each brain area is represented as a local network composed by excitatory (E) and inhibitory (I) neural populations coupled by pathways of NMDA and GABA synapses. The excitatory synaptic coupling (J_{NMDA}) goes from the excitatory to the inhibitory population and is NMDA mediated, as well as the local recurrent excitation (w_+), while the feedback inhibitory coupling (J_i) is GABAergic. The structural connectivity matrix weights inter-areal connections and is scaled by the global coupling G. Brain dynamics are described by a set of coupled non-linear stochastic differential equations, in which where $r_i^{(E,I)}$ denotes the firing rate of the excitatory and inhibitory populations, $S_i^{(E,I)}$ identifies the average excitatory or inhibitory synaptic gating variables at local area, i, and $I_i^{(E,I)}$ is the input current to the excitatory and inhibitory populations at local area, i.

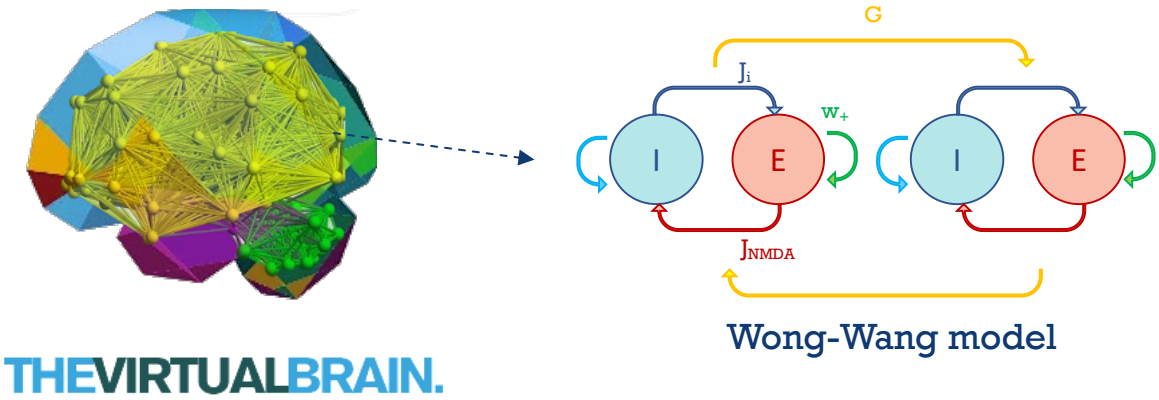

Model Parameters (Wong-Wang)

$$I_i^{(E)} = W_E I_0 + w_+ J_{NMDA} S_i^{(E)} + G J_{NMDA} \sum_j C_{ij} S_j^{(E)} - J_i S_i^{(I)} \quad (1)$$

$$I_i^{(I)} = W_I I_0 + J_{NMDA} S_i^{(E)} - S_i^{(I)} \quad (2)$$

$$r_i^{(E)} = H^{(E)}\left(I_i^{(E)}\right) = \frac{a_E I_i^{(E)} - b_E}{1 - \exp\left(-d_E\left(a_E I_i^{(E)} - b_E\right)\right)} \quad (3)$$

$$r_i^{(I)} = H^{(I)}\left(I_i^{(I)}\right) = \frac{a_I I_i^{(I)} - b_I}{1 - \exp\left(-d_I\left(a_I I_i^{(I)} - b_I\right)\right)} \quad (4)$$

$$\frac{d S_i^{(E)}(t)}{dt} = -\frac{S_i^{(E)}}{\tau_E} + \left(1 - S_i^{(E)}\right)\gamma r_i^{(E)} + \sigma \upsilon_i(t) \quad (5)$$

$$\frac{d S_i^{(I)}(t)}{dt} = -\frac{S_i^{(I)}}{\tau_I} + r_i^{(I)} + \sigma \upsilon_i(t) \quad (6)$$

Supplementary Figure 2| Parameter space exploration. Parameter space exploration is conducted in two steps: first, G and J_i are optimized with the other two parameters (J_{NMDA} and w_+) at their standard value; then J_{NMDA} and w_+ are optimized with G and J_i fixed at their optimized value. Heat maps represent the value of the cost function obtained with different parameters combinations. Optimal parameters are the ones leading to the lowest cost function between simulated and experimental data.

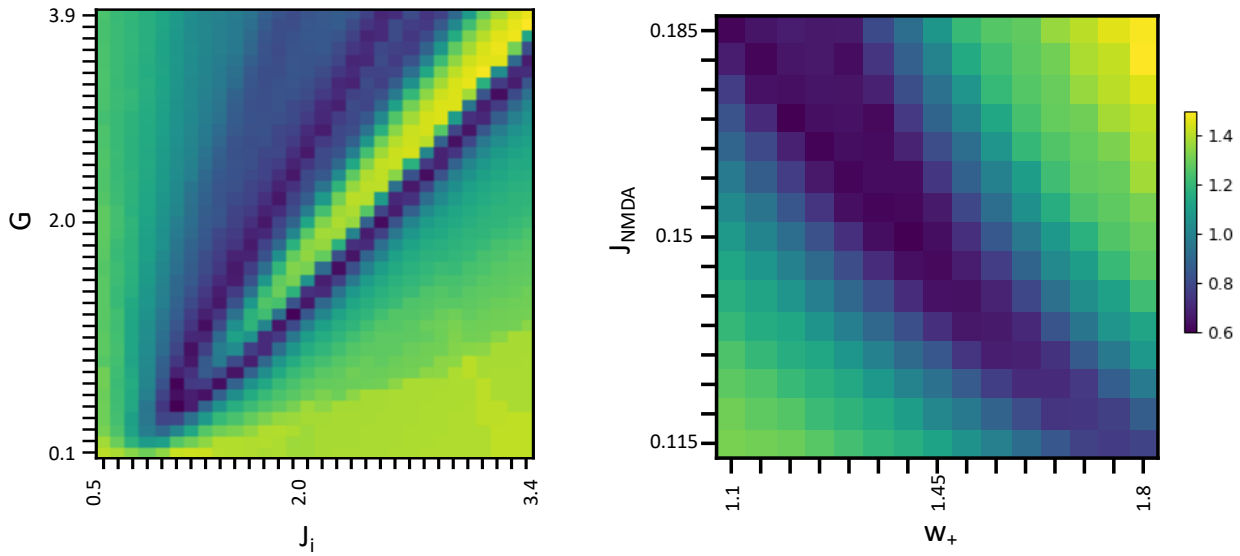

Supplementary Figure 3| Feature importance distribution according to F1 score (x axis) given by the random forest (RF) ranking in 100 iterations on graph theory measures after splitting the data into 70% for training and 30% for testing. The first five non correlated (spearman test) features were selected as inputs to the subsequent clustering analysis. The emerging features belong to the LN, AN and SMN networks and are shown as underlined.

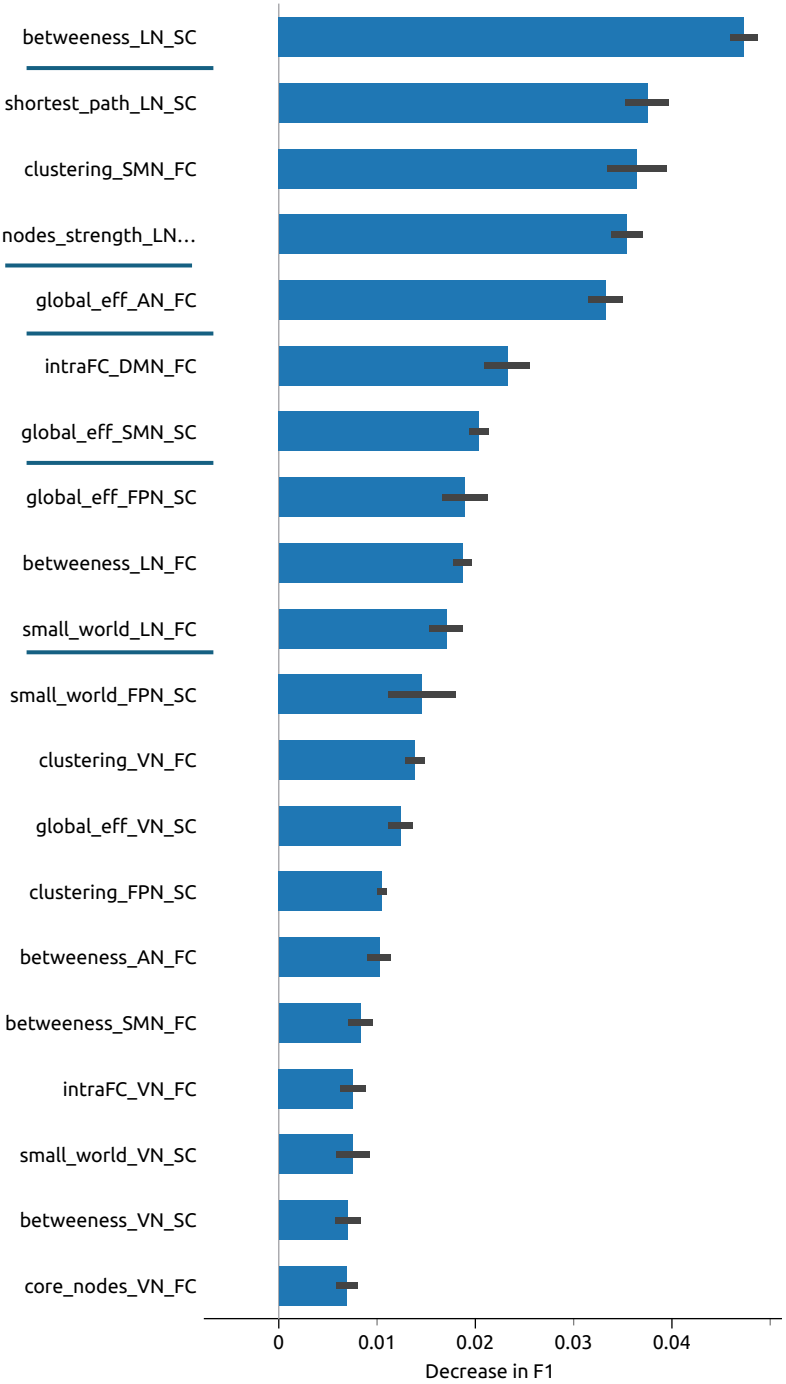

Supplementary Figure 4| Visual representation of subjects' distribution in the clusters (different colors) found using the meaningful topological features of LN, AN and SMN identified with random forest. Different shapes reflect different clinical groups (HC, MCI, AD). The mean Silhouette values of each cluster are: Ct1 – 0.215, Ct2 – 0.126, Ct3 – 0.236.

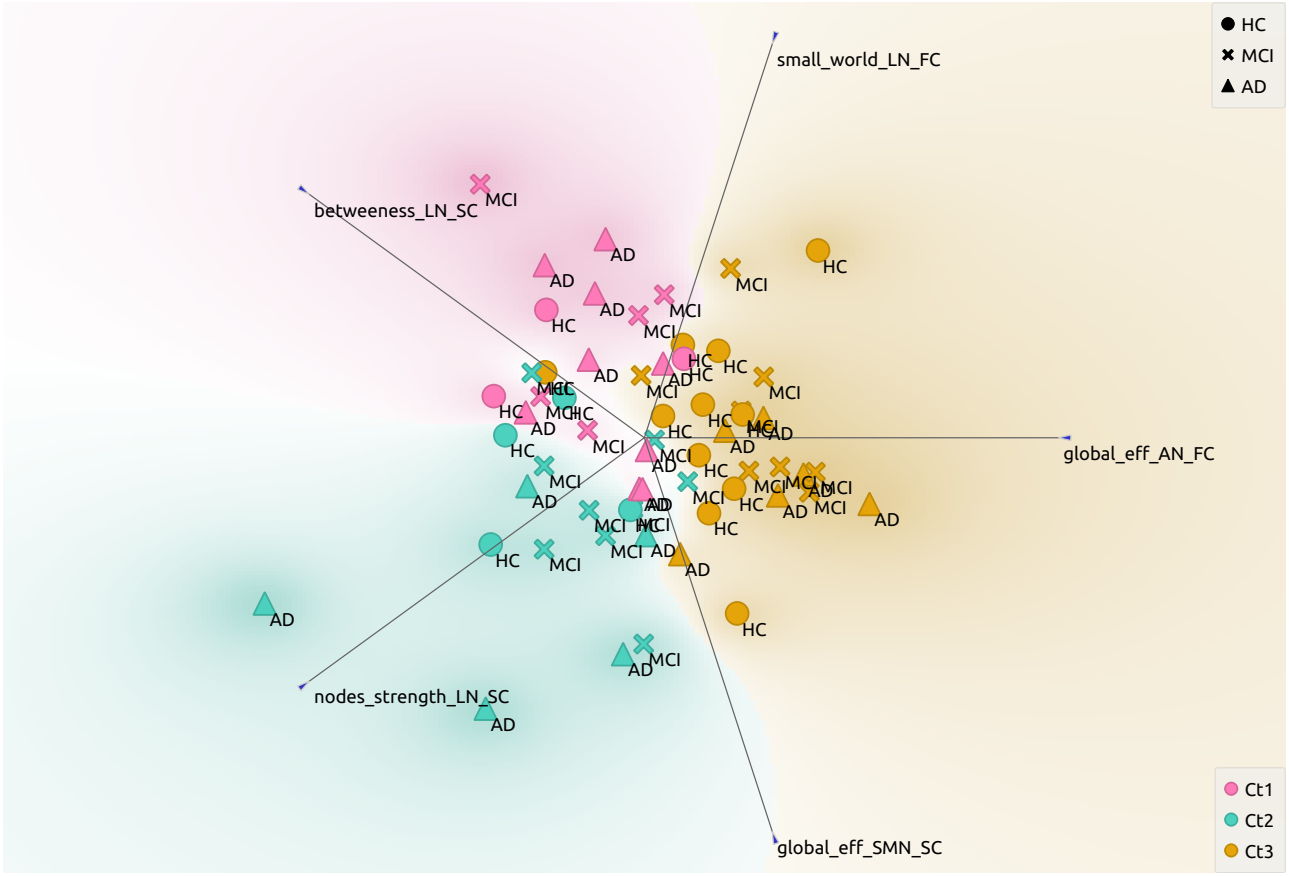

Supplementary Figure 5| Feature importance distribution according to F1 score (x axis) given by random forest (RF) ranking in 100 iterations on TVB parameters after splitting the data into 70% for training and 30% for testing. The first five non correlated (spearman test) features were selected as inputs to the subsequent clustering analysis. The emerging features belong to both cognitive and motor networks and are shown as underlined.

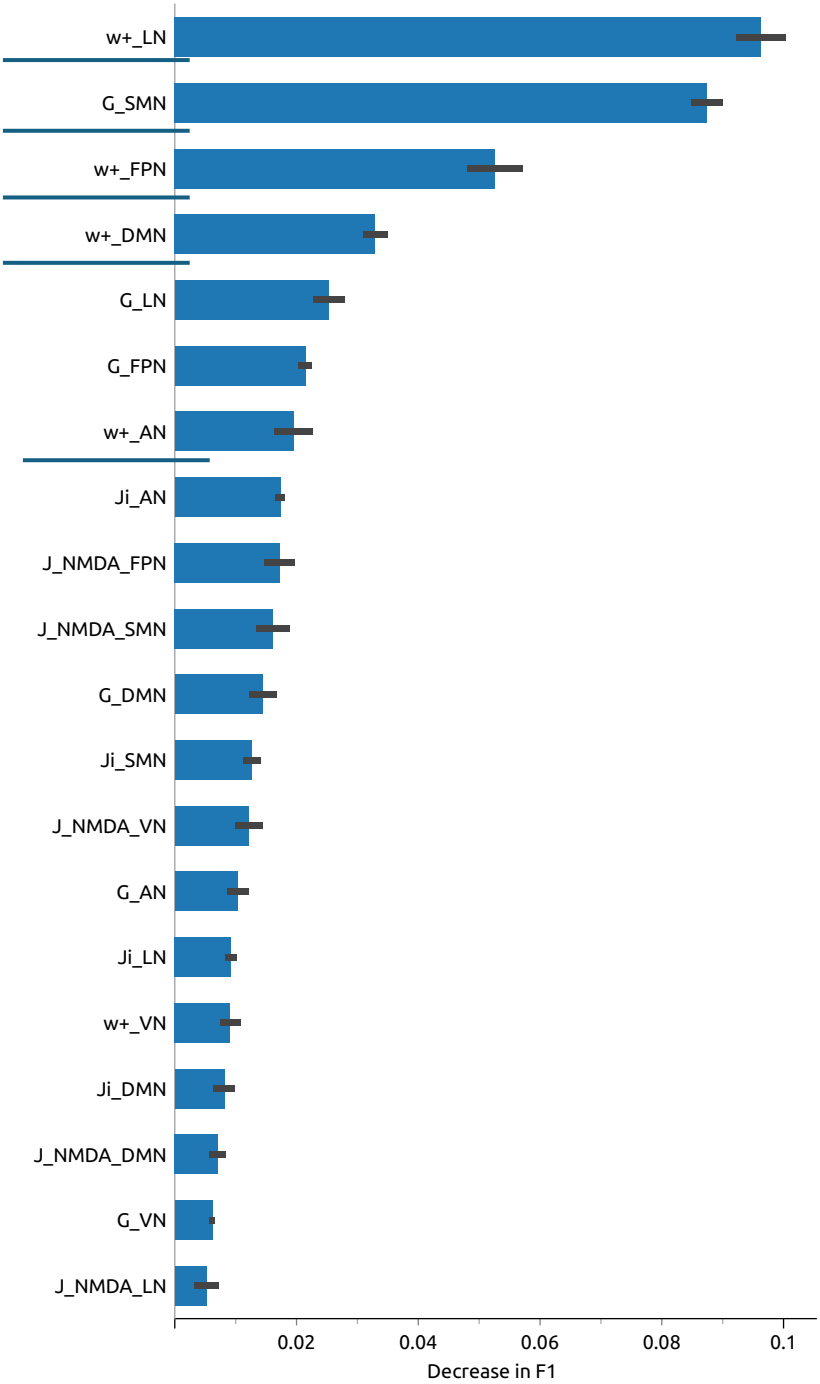

Supplementary Figure 6| Visual representation of subjects' distribution in the clusters (different colors) found using the meaningful TVB features of brain networks identified with random forest. Different shapes reflect different clinical groups (HC, MCI, AD). The mean Silhouette values of each cluster are: Cd1 - 0.098, Cd2 - 0.266, Cd3 - 0.213.

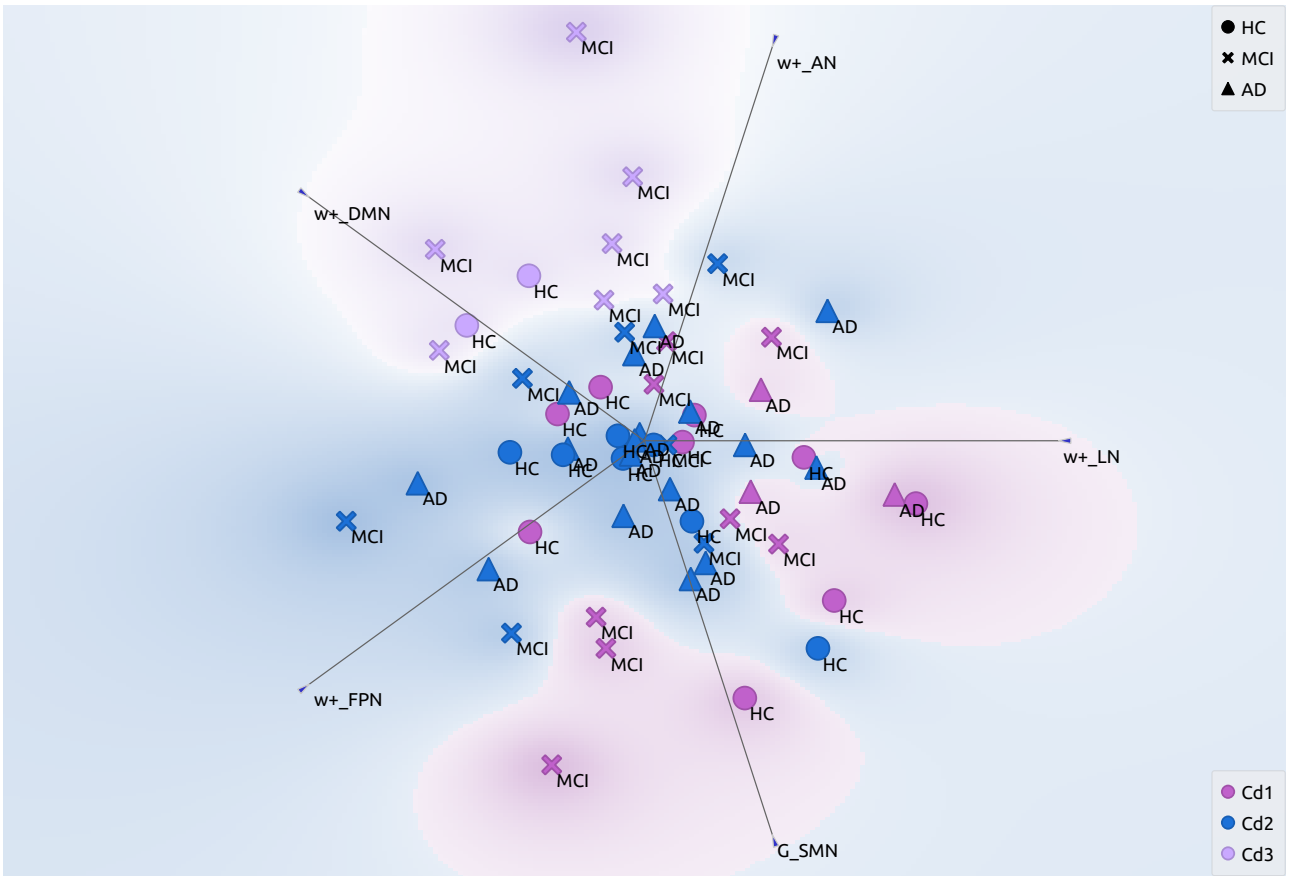

Supplementary Figure 7| Explanatory SC and FC matrices

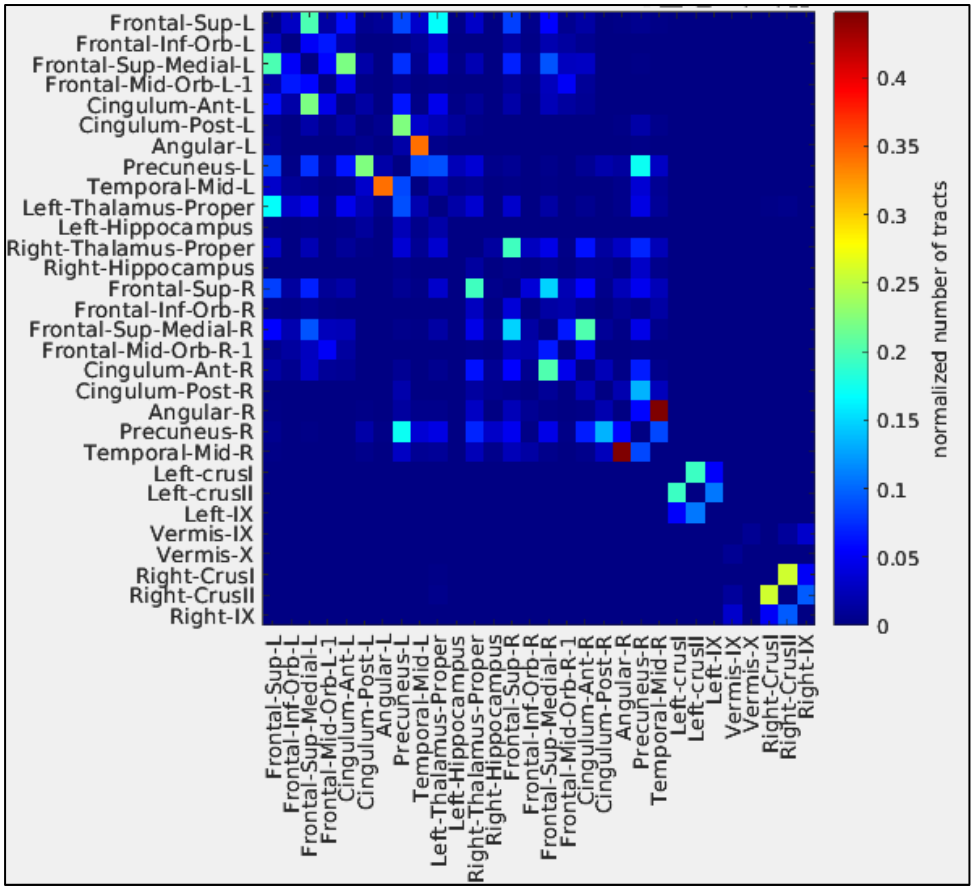

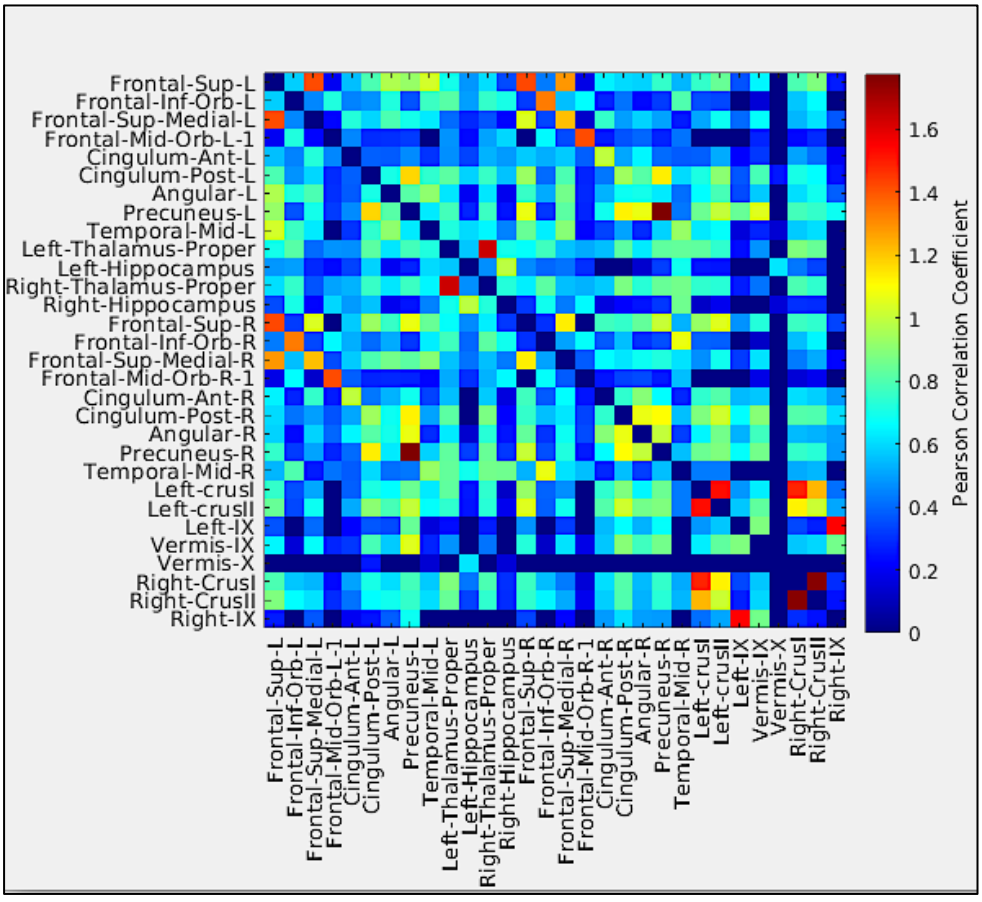

Supplementary Table 1: Demographics, clinical and neuropsychological data.

Measures	HC	MCI	AD
Males/females	9/9	8/14	4/16
Age (years)	69 (5)	75 (6)	71 (7)
Verbal episodic memory	-	1.3 (1.5)	0.3 (0.7)
Visuoconstructional abilities	-	2.5 (1.3)	1.5 (1.7)
Spatial episodic memory	-	1.8 (1.5)	0.6 (1.2)
Verbal short term memory	-	2.8 (1.2)	3 (1.3)
Semantic fluency	-	2.3 (1.4)	1.4 (1.3)
Lexical retrieval	-	2.7 (1.2)	2.7 (1.4)
Attentional shifting	-	1.4 (1.6)	1.2 (1.4)
Verbal working memory	-	3 (0.9)	2.1 (1.4)

Supplementary Table 2: Wong-Wang model parameters.

PARAMETERS	VALUE	DESCRIPTION
a_E, b_E, d_E, τ_E, W_E	310 nC^{-1}, 125 Hz, 0.16 s, 100 ms, 1	Excitatory gating variables
a_I, b_I, d_I, τ_I, W_I	615 nC^{-1}, 177 Hz, 0.087 s, 10 ms, 0.7	Inhibitory gating variables
γ	0.641/1000	Kinetic parameter
σ	0.01 nA	Noise amplitude
I_0	0.382 nA	Overall effective external input
C_{ij}	Obtained from diffusion tractography	Structural connectivity (SC) matrix
G	Obtained from parameters optimization	Global coupling scaling factor
J_i	Obtained from parameters optimization	Feedback inhibitory synaptic coupling
J_{NMDA}	Obtained from parameters optimization	Excitatory synaptic coupling
w_+	Obtained from parameters optimization	Local excitatory recurrence

Supplementary Methods

MRI acquisition

The MRI acquisitions were performed using a 3T Siemens Skyra scanner with a 32-channel head coil and included diffusion weighted imaging (DWI) and resting-state fMRI (rs-fMRI) scans[1]. For DWI data, an axial double-shell single-shot Spin Echo (SE) - Echo-Planar Imaging (EPI) was performed (voxel size = 2.5 x 2.5 x 2.5 mm^3, TR/TE = 8400/93 ms, two shells with 30 isotropically distributed diffusion-weighted directions, diffusion weightings of 1000 and 2000 s/mm^2, 7 non-diffusion weighted images (b = 0 s/mm^2, b_0 images)). Three non-diffusion weighted images were acquired with a reversed phase-encoding for distortion correction. For rs-fMRI data, an axial Gradient Echo (GE) EPI sequence (voxel size = 3 x 3 x 3 mm^3, TR/TE = 2400/30 ms, 200 volumes) was used. For anatomical reference, the protocol included a high-resolution 3D sagittal T1-weighted (3DT1) scan (TR/TE = 2300/2.96 ms, TI = 900 ms, flip angle = 9°, in-plane resolution = 1 x 1 mm, slice thickness = 1 mm).

Preprocessing of DWI and rs-fMRI data

Preprocessing of diffusion and fMRI data was performed according to[2,3]. DWI data were denoised and corrected for motion and eddy currents distortion[4] (FMRIB Software Library, FSL). White matter, gray matter (GM), subcortical GM and CSF were segmented from the co-registered 3DT1 volume[5] (MRtrix3) and a 30 million streamlines whole-brain anatomically constrained tractography[6] was performed, estimating fiber orientation with multi-shell multi-tissue constrained spherical deconvolution (CSD) and using probabilistic streamline tractography[7]. fMRI preprocessing was carried out combining SPM12 (Welcome Department of Cognitive Neurology), FSL and MRtrix3 commands in a custom MATLAB script (v2019b, The MathWorks, Natick, Mass). Marchenko-Pastur principal component analysis (MP-PCA) denoising[8] was performed, followed by slice-timing correction, realignment, co-registration to the 3DT1 volume, polynomial detrending, nuisance regression of 24 motion parameters[9] and CSF temporal signal[10], and temporal band-pass filtering (0.008-0.09 Hz).

Structural and functional connectivity

To consider both cerebral cortical and subcortical regions and cerebellar regions, an ad-hoc gray matter parcellation atlas was created combining 93 cerebral (AAL) and 33 cerebellar (SUIT) labels[11,12]. For each subject, structural (SC) and functional connectivity (FC) were reconstructed applying the parcellation atlas to whole-brain tractography, and rs-fMRI. The parcellation atlas applied to whole-brain tractography generated two types of matrices: a distance matrix containing the lengths of the tracts connecting each pair of nodes, and a weight matrix in which the normalized number of streamlines represents the connection strength. From rs-fMRI data, the time-course of the BOLD signal was obtained for each node. To identify the gray matter nodes belonging to the six main functional brain networks, a mapping between our atlas and the ones by Buckner (cerebellar) and Yeo (cerebral)[13,14] was performed. Indeed, these two functional atlases identify six networks known to support specific functions: i) integrative functions: default mode network (DMN), frontoparietal network (FPN), limbic network (LN), attention network (AN); ii) motor and sensory functions: visual network (VN), somatomotor network (SMN). The subset of nodes defining each network and their connections were extracted from whole-brain SC obtaining specific network SC matrices, used as input to TVB (as detailed below). Static and dynamic experimental FC (expFC and expFCD,) for each of the six brain networks were reconstructed to capture both synchronous BOLD signal fluctuations BOLD and their spatiotemporal-dynamics in resting-state[15]. Static functional connectivity was calculated with the Pearson Correlation Coefficient (PCC) between node pairs and the PCC matrix was thresholded at 0.0126 after a Fisher's z transformation[16]. The FCD matrix was obtained by a FC computed over a sliding window of 40 seconds with incremental shifts of 1 TR[17] followed by the estimation of FCD as a time-versus-time matrix, incorporating the correlation between the FC at different time points, and quantifying the time-evolving dynamics.

Definition of topological measures

For each subject, the main GT metrics (Brain Connectivity Toolbox, Matlab) were obtained from static FC and SC matrices of resting state brain networks. Following the general definitions[18], the parameters for describing the nodes in the networks were the density and the core nodes. Networks density was computed as mean nodal degree, defined as the fraction of actual connections with respect to possible connections. Nodes presenting the maximum numbers of connections were defined as core nodes and considered as mostly involved in signal transmission. For the SC matrix nodes strength and the shortest path were also computed, to quantify the distance and the strength of connections between a node and its neighbors. For the FC matrix intraFC was estimated as the mean of the functional weights between nodes, to quantify the strength of functional connections. Structural and functional networks integration and segregation were evaluated, respectively, with global efficiency and clustering coefficient values. Global efficiency is inversely related to

topological distance between nodes and generally reflects the ability to efficiently combine information from different connected regions. Clustering coefficient quantifies the inclination of the nodes in a graph to reorganize in clusters. Combining the length of paths with the clustering coefficient measures, it was possible to define whether a network exhibits small-world properties. Small-worldness reflects the tendency of a network to balance local segregation with long-distance integration and small world networks are characterized by high clustering coefficient and short characteristic path length. As a measure of nodes centrality the betweenness centrality was computed from path lengths.

Statistics and machine learning

Statistical tests were performed using IBM-SPSSv.21. First, GT measures and TVB parameters for each network were tested for normality (Shapiro-Wilk, $p<0.05$). Then, a multivariate general linear model (GLM) followed by post-hoc Bonferroni correction was applied to detect network topology and excitation/inhibition differences between groups correcting for age and gender differences between the groups.

To reduce the parameter space, a machine learning pipeline was implemented in Orange 3.36.2. and applied to both GT measures and TVB parameters. The parameters of interest (either GT or TVB) from all subjects were normalized and given as input to a decision-tree-based Random Forest algorithm that performed a feature selection to extract the parameters that best separated the three clinical groups AD, MCI, and HC, while avoiding overfitting. A Random Forest algorithm with ten-trees performed the features ranking in 100 iterations after splitting the data into 70% for training and 30% for testing, and the F1 score was used to evaluate the relevance of the features. The top five uncorrelated (Spearman test) features were used as input for the clustering analysis. The Silhouette test, performed with ten permutations, was used to determine the optimal number of clusters, and the K-means method was used to assign subjects to clusters. Differences in parameters between clusters were assessed using a multivariate general linear model. *A posteriori* analysis of subjects' distributions between clusters was conducted to check the correspondence between topology/dynamics and Aβ and τ biomarkers positivity/MMSE scores of MCI patients. Multiple regression analysis was performed to explore the relationship between the neuropsychological assessment of each cognitive domain and the combination of GT and TVB parameters. The regression was performed in a backward approach, using neuropsychological scores as dependent variables, and considering as predictors in turns: (i) GT parameters alone, (ii) TVB parameters alone and (iii) both GT and TVB measures. The regression algorithm automatically removed predictors until selecting the significant ones (F test, $p<0.05$) explains the neuropsychological scores variance.

References

1. Nigri, A. *et al.* Quantitative MRI Harmonization to Maximize Clinical Impact: The RIN–Neuroimaging Network. *Front. Neurol.* **13**, (2022).
2. Monteverdi, A. *et al.* Virtual brain simulations reveal network-specific parameters in neurodegenerative dementias. *Front. Aging Neurosci.* **15**, 1–15 (2023).
3. Monteverdi, A. *et al.* Subject-specific features of excitation / inhibition profiles in neurodegenerative diseases. *Front. Aging Neurosci. 14868342.* (2022) doi:10.3389/fnagi.2022.868342.
4. Andersson, J. L. R. & Sotiropoulos, S. N. An integrated approach to correction for off-resonance effects and subject movement in diffusion MR imaging. *Neuroimage* **125**, 1063–1078 (2016).
5. Patenaude, B., Smith, S. M., Kennedy, D. N. & Jenkinson, M. A Bayesian model of shape and appearance for subcortical brain segmentation. *Neuroimage* **56**, 907–922 (2011).
6. Smith, R. E., Tournier, J. D., Calamante, F. & Connelly, A. Anatomically-constrained tractography: Improved diffusion MRI streamlines tractography through effective use of anatomical information. *Neuroimage* **62**, 1924–1938 (2012).
7. Tournier, J. D., Calamante, F. & Connelly, A. MRtrix: Diffusion tractography in crossing fiber regions. *Int. J. Imaging Syst. Technol.* **22**, 53–66 (2012).
8. Ades-Aron, B. *et al.* Improved task-based functional MRI language mapping in patients with brain tumors through marchenko-pastur principal component analysis denoising. *Radiology* **298**, 365–373 (2020).
9. Friston, K. J., Williams, S., Howard, R., Frackowiak, R. S. J. & Turner, R. Movement-related effects in fMRI time-series. *Magn. Reson. Med.* **35**, 346–355 (1996).
10. Muschelli, J. *et al.* Reduction of motion-related artifacts in resting state fMRI using aCompCor. *Neuroimage* **96**, 22–35 (2014).
11. Tzourio-Mazoyer, N. *et al.* Automated anatomical labeling of activations in SPM using a macroscopic anatomical parcellation of the MNI MRI single-subject brain. *Neuroimage* **15**, 273–289 (2002).
12. Diedrichsen, J., Balsters, J. H., Flavell, J., Cussans, E. & Ramnani, N. A probabilistic MR atlas of the human cerebellum. *Neuroimage* **46**, 39–46 (2009).
13. Thomas Yeo, B. T. *et al.* The organization of the human cerebral cortex estimated by intrinsic functional

connectivity. *J. Neurophysiol.* **106**, 1125–1165 (2011).
14. Buckner, R. L., Krienen, F. M., Castellanos, A., Diaz, J. C. & Thomas Yeo, B. T. The organization of the human cerebellum estimated by intrinsic functional connectivity. *J. Neurophysiol.* **106**, 2322–2345 (2011).
15. Hansen, E. C. A., Battaglia, D., Spiegler, A., Deco, G. & Jirsa, V. K. Functional connectivity dynamics: Modeling the switching behavior of the resting state. *Neuroimage* **105**, 525–535 (2015).
16. Palesi, F. *et al.* The Importance of Cerebellar Connectivity on Simulated Brain Dynamics. *Front Cell Neurosci* **14**, 1–11 (2020).
17. Battaglia, D. *et al.* Dynamic Functional Connectivity between order and randomness and its evolution across the human adult lifespan. *Neuroimage* **222**, 117156 (2020).
18. Rubinov, M. & Sporns, O. Complex network measures of brain connectivity: Uses and interpretations. *Neuroimage* **52**, 1059–1069 (2010).